Development and Characterization of $CD4^+$ T Cell Targeting Nanoparticles for Therapeutic Delivery of Immunomodulatory Drugs

By

Christopher Paul Haycook

Thesis

Submitted to the Faculty of the

Graduate School of Vanderbilt University

in partial fulfillment of the requirements

for the degree of

Master of Science

in

Biomedical Engineering

December 15, 2018

Nashville, Tennessee

Approved:

Todd D. Giorgio, Ph.D.

Amy S. Major, Ph.D.

ACKNOWLEDGEMENTS

I would like to thank my advisor Dr. Todd Giorgio and collaborating faculty members Dr. Amy Major and Dr. Charles Hong for their support throughout this work. Thanks to Dr. Giorgio, Dr. Major, and Dr. Hong for conceiving the original research idea, for providing scientific guidance on this project, and for pushing me to overcome the many exciting challenges and conundrums that scientific research has to offer. I would also like to thank several members of the Giorgio, Major, Hong, and Duvall laboratories for their help through this project. Thanks to Isom Kelly for providing training to perform sonication mediated nanoparticle synthesis protocols. Thanks to Evan Glass for conducting many of the preliminary experiments and data collection with me leading up to the work presented in my thesis. Thanks to Charles Williams for providing the eggmanone used in all experiments presented herein. Thanks to Jillian Rhoads for conducting flow cytometry analysis and ELISAs during the preliminary phase of this project. Thanks to Joe Balsamo for conducting ELISAs, flow cytometry analysis, and additional pharmacological and immunological experiments characterizing eggmanone in tandem with nanoparticle development. Thanks to my undergraduate colleague Carla Pax for performing nanoparticle synthesis and characterization that supported the work presented herein. Thank you to my undergraduate mentor, Dr. M. Robert Gower, for providing the initial research training that motivated me to pursue biomedical engineering graduate research. Lastly, I would like to thank my friends and family for supporting me throughout my graduate education.

TABLE OF CONTENTS

LIST OF FIGURES

CHAPTER I

BACKGROUND

Systemic Lupus Erythematosus

The primary focus of this research is the development of a nanoparticle delivery vehicle capable of specifically delivering hydrophobic immunomodulatory drugs to T cells. T cell activity is dysregulated in a variety of autoimmune diseases with limited therapeutic options available other than overt immunosuppression. Numerous immunomodulatory compounds have been developed in order to combat T cell hyperactivity, however, many are hydrophobic and require a carrier to enable clinical translation.[1] Thus, the delivery of hydrophobic drugs to T cells is an unmet clinical need. One such disease that could benefit from novel therapeutics such as eggmanone, whose clinical potential is limited by rapid excretion, is systemic lupus erythematosus (SLE).

Lupus is an autoimmune disease that affects nearly 5 million people worldwide with an incidence rate of nearly 16,000 new cases each year in the United States.[2,3] SLE is the most common form of the disease, accounting for ~70% of all cases. Nearly half of all patients with SLE experience some detrimental effect on major organs including the heart, lungs, kidneys, or brain, and many suffer from multiple autoimmune diseases.[3,4] The majority of patients affected by SLE are young women, especially those with African American heritage.[4]

SLE pathophysiology consists of chronic autoreactive T and B cell hyperactivity that leads to antibody production against self-antigens and widespread inflammation, resulting in chronic pain and the potential for organ failure. The majority of treatments for patients with SLE are focused on managing inflammation through suppression of their immune systems.[5] Although

these therapies can be effective in minimizing the symptoms of the disease, they do not address the cause, and 10-15% of patients die prematurely resulting from complications[6], including opportunistic infections due to immunosuppression. Moreover, patients are often not correctly diagnosed with lupus until 6 years after first experiencing symptoms because they resemble a number of other diseases.[7]

The primary symptoms of SLE usually present in patients as periodic "flares" of varying intensity. This unpredictable, wavelike behavior of symptom intensity is the result of antinuclear antibody mediated immune responses against antigens associated with apoptosis. Apoptotic antigens are released following triggering events including periods of emotional and physical stress, ultraviolet radiation, infection, and others.[5] As apoptosis occurs, nuclear material is released into the surrounding tissues and eventually enters the bloodstream. During a "flare", antinuclear antibodies bind to nuclear material in the blood and tissues including: DNA, RNA, anionic phospholipids, histones, and ribonucleoproteins. Molecular structures consisting of soluble antigen bound to antibodies, known as immune complexes, are formed in large amounts, deposit in tissues, and lead to tissue damage by activation of the complement cascade and recruitment of inflammatory cells.[8] Immune complexes often circulate in the blood and accumulate in the kidney due to electrostatic interactions between cationic antinuclear antibodies and the anionic regions of the kidney glomeruli, where they can lead to organ failure. Additionally, autoantibodies can interfere with coagulation, aggregate platelets, and bind to ischemic tissues leading to T cell infiltration, inflammatory cytokine production, and additional tissue damage.[8]

Common therapeutic strategies to manage disease symptoms include: nonsteroidal anti-inflammatory drugs (NSAIDs), antimalarial medication, steroids, immunosuppressants, and

monoclonal antibodies. NSAIDs are prescribed to manage chronic pain and swelling, but they can lead to gastrointestinal, renal, and hepatic toxicity if used for prolonged periods. Antimalarial medications, such as hydroxychloroquine are thought to interfere with T cell activation and production of inflammatory cytokines, however, their mechanism of action is not completely understood, and they have the potential to cause serious macular damage and muscle weakness. Corticosteroids suppress inflammatory immune cell function, but lead to serious long-term side effects including edema, growth suppression, increased risk of infections, and hypertension. Immunosuppressants, such as cyclophosphamide and azathioprine function to suppress T and B cell proliferation during severe "flares", but can lead to renal dysfunction, increased risk of infection, infertility, and cancer. Monoclonal antibodies such as Rituximab and Belimumab, the first agent approved by the FDA for the treatment of lupus in over 50 years, function to inhibit survival of autoantibody producing B cells at the cost of leading to nausea, extremity pain, and infections of the respiratory and urinary systems.[5,8–10]Although all of these strategies can alleviate symptoms, every one of them has the potential to cause harmful side-effects that necessitate the development of more effective therapeutics as the core disease mechanisms of SLE are elucidated.

Germinal Center Immunology

Although SLE is mainly thought of as an antibody mediated disease, the production of IgG antibodies, the isotype with the highest antigen affinity and plasma circulation potential, is a T cell dependent process that is regulated in germinal center responses. The germinal center response is a highly orchestrated event involving germinal center B cells, T follicular helper cells, and follicular dendritic cells, that regulates B cell antibody affinity maturation and isotype

switching in secondary lymphoid organs (Figure 1). Germinal center responses begin when naïve T and B cells specific for the same antigen are activated by antigen presenting dendritic cells, and B cell receptor (BCR) binding of soluble antigen, in the T and B cell zones respectively.[11–13] Once activated, $CD4^+$ T cells expressing CD154 interact with their equivalent B cells that express CD40 at the boundary of the T and B cell zones to initiate the germinal center response.[14] At this time, a portion of these T cells mature into T follicular helper cells, migrate to the germinal center to interact with follicular B cells, and initiate the germinal center response.

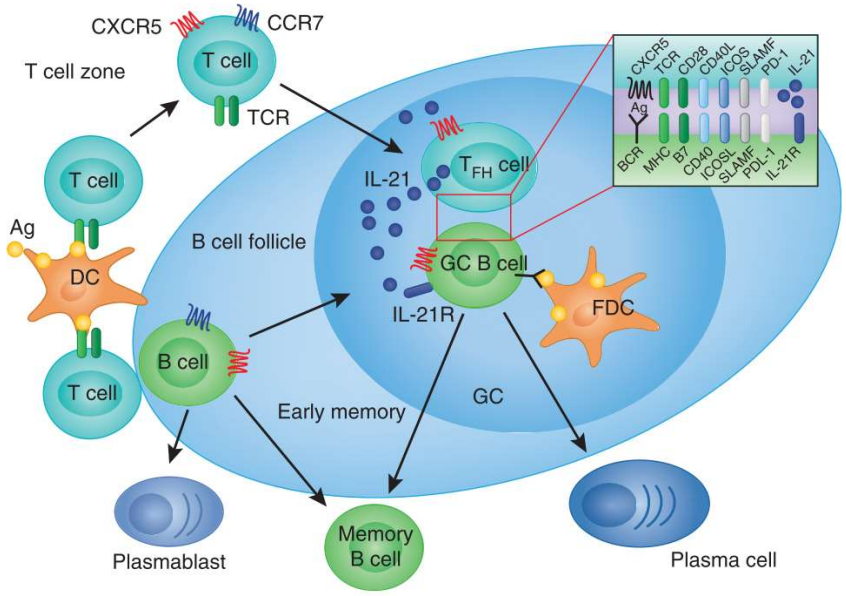

Figure 1: ***Schematic Representation of the Germinal Center Response.*** Figure from.[13]

The germinal center is divided into two regions known as the dark zone and the light zone. In the dark zone, activated follicular B cells rapidly proliferate and undergo somatic

hypermutation processes that introduce mutations in the antigen binding site of the BCR, known as the variable region, that can result in higher affinity antibody potentials. In the light zone, T follicular helper cells and follicular dendritic cells interact with B cells exiting the dark zone in order to supply survival signals to B cells producing antibodies with the highest affinity for a given antigen, a process known as affinity maturation. Additionally, cytokine signaling provided by T follicular helper cells can stimulate follicular B cells to produce antibodies with isotypes other than IgM in a process known as immunoglobulin class switching.[11–13] The isotype of an antibody determines its effector function through interaction with Fc receptors on the surface of immune cells, as well as its pharmacokinetic properties.[15] At the end of the germinal center response, long-lived high affinity antibody secreting plasma cells exit the germinal center and travel to the bone marrow to produce antibody.[11–13]

Unfortunately, the somatic hypermutation, affinity maturation, and class switching processes that occur in the germinal center provide the pathogenic potential of *de novo* generation of autoantibodies that potentiate inflammation in SLE. In fact, it has been reported that T and B cells in the periphery of patients with active SLE spontaneously express CD154, suggesting that germinal center responses are overactive in patients during a "flare".[14] Moreover, some of the most common autoantibodies produced by patients with SLE are specific for nuclear peptides, such as histones and ribonucleoproteins, both of which are T cell dependent antigens. Preventing the activation of autoreactive $CD4^+$ T cells involved in the germinal center response may, therefore, interfere with abnormal B cell activation associated with active SLE.

CHAPTER II

INTRODUCTION

Synthetic Particulate Delivery Systems for T Cell Modulation

A variety of leukocytes, including antigen presenting cells (APCs), frequently sample their environment for potential pathogens, as well as dead or dying cells, in a process known as professional phagocytosis. Professional phagocytes utilize surface bound receptors to detect and efficiently engulf pathogens before communicating their presence to the adaptive immune system. Knowledge of the mechanisms that control this process have enabled the delivery of a variety of immunomodulatory agents, most notably those used as vaccine adjuvants, to APCs. However, T cells primarily rely on communication mechanisms consisting of physical connection with APCs, and soluble cytokine signaling, rather than phagocytosis to perform effector functions. Thus, a variety of synthetic nanoengineered particulate systems have been developed in order to overcome the inability of T cells to perform professional phagocytosis so that immunomodulatory cargo can be delivered.

Synthetic particulate systems can provide targeting and delivery of intracellular signals to T cells through conjugation of ligands to the surface, or encapsulation of cargo within particulate systems, respectively.[16] Polyplex micellular nanoparticles composed from amphiphilic polymers that electrostatically complex with siRNA were used to silence inflammatory genes in activated T cells.[17] However, the stability of injected micellular delivery systems is largely dependent on the critical micelle concentration (CMC), which determines the necessary concentration of a specific amphiphilic polymer needed to spontaneously form micelles.[18] Once intravenously

injected, the concentration of micelles can quickly fall below their CMC as they disperse within circulating serum, leading to premature release of cargo. Although enormous scientific effort has been invested to develop novel polymers with CMCs appropriate for systemic delivery, their clinical translation has been hindered by the cost of synthesis, as well as FDA regulatory approval processes that establish safety. Liposomal delivery systems have also been developed to deliver immunomodulatory drugs to T cells.[19] However, the carrying capacity of hydrophobic agents is dependent on the available volume within the lipid bilayer that composes these particles. Consequentially, the individual payload of nano-sized liposomes is limited compared to nano-emulsion particulate systems made from polymers such as poly(lactic-co-glycolic acid) (PLGA). In fact, 14 PLGA particulate drug delivery systems are currently FDA approved and available for use in the US. Nevertheless, none are approved for systemic delivery.[20]

Hedgehog Signaling in Immunity and the Discovery of Eggmanone

The Hedgehog signaling (Hh) pathway is traditionally associated with regulation of cell differentiation mechanisms in the development of the embryo of vertebrates.[21] However, it has also been shown to play a key role in the differentiation and maturation of lymphocytes. In the thymus, developing T cell clones undergo central tolerance mechanisms including positive and negative selection. Positive selection ensures that the T cell receptor (TCR) can interact with the major histocompatibility complex (MHC) molecules of antigen presenting cells. Negative selection is responsible for deleting T cell clones with TCRs that are specific for self-antigen. Recently, it was discovered that insufficient Hh signaling in the thymus can lead to increased negative selection, while overactivation can lead to decreased negative selection and the escape of autoreactive T cell clones.[22]

In the periphery, Hh signaling has also been implicated in regulating the activation of T and B lymphocytes. Three signals are provided by antigen presenting cells in order to activate a naïve T cell clone: binding of the TCR with peptide bound MHC, binding of membrane bound co-stimulatory molecules with their respective receptors, and soluble cytokine signals. Recently, Chan *et al.* discovered that Hh signaling proteins are able to provide co-stimulatory effects to $CD4^+$ T cells that promote proliferation and cytokine production. Interestingly, these effects were strongest at sub-optimal TCR stimulation levels, and appear to activate gene expression regulated by CD28[23], a costimulatory molecule that is commonly targeted for inhibition in the treatment of rheumatic autoimmunity.[24] Furthermore, Hh signaling proteins have also been shown to be produced by follicular dendritic cells in the germinal center in order to inhibit Fas-mediated apoptosis of B cells[25], an important mechanism that regulates the elimination of autoreactive B cells.[26]

Eggmanone is a small molecule inhibitor of the Hh signaling pathway that was discovered at Vanderbilt University.[27] Unlike commercially available small molecule Hh inhibitors that specifically inhibit the upstream G protein-coupled receptor Smoothened (SMO), and are susceptible to acquired resistance, eggmanone antagonizes phosphodiesterase 4 (PDE4), a downstream regulator of Hh gene transcription. Importantly, unlike other PDE4 inhibitors, eggmanone inhibits PDE4 by raising cyclic AMP locally, instead of raising total cellular cyclic AMP content.[27] If delivered to the germinal center, eggmanone could potentially inhibit autoimmune lymphocyte survival through suppression of Hh mediated costimulatory and anti-apoptotic effects on $CD4^+$ T cells and B cells, respectively. However, eggmanone is also extremely hydrophobic, leading to rapid excretion and ineffective intravenous administration without encapsulation within a rationally designed delivery vehicle.

Nanoparticle Delivery of Hydrophobic Immunotherapeutics to CD4$^+$ T Cells

Previous attempts to specifically deliver hydrophobic immunomodulatory cargo to CD4$^+$ T cells have utilized several PLGA nanoparticle formulations to create localized drug delivery depots at the cell surface. McHugh *et al.* conjugated biotin labeled whole αCD4 antibodies to avidin coated PLGA nanoparticles capable of hydrophobic drug delivery.[28] Although they were able to achieve high targeting specificity in CD4 targeted particles, compared to isotype control particles *ex vivo*, avidin and streptavidin conjugation systems have previously been shown to be immunogenic, and could therefore exacerbate the already highly inflammatory immune environment associated with autoimmunity.[29] Additionally, conjugation of whole targeting antibodies that contain foreign Fc regions can lead to rapid clearance of nanoparticles in systemic circulation via Fc receptor mediated clearance by the reticuloendothelial system (RES), which may explain why no intravenous administrations were evaluated.[30] Cao *et al.* utilized maleimide-thiol conjugation of αCD4 antibody fragments to PLGA nanoparticles coated with lipid-polyethylene glycol (lipid-PEG) (fCD4-LCNPs). This formulation decreased the potential of opsonization mediated clearance by the RES through incorporation of hydrophilic PEG[30], and also provided tunable control of nanoparticle surface charge via mixing of cationic and anionic lipids in the surface coating. Although this formulation incorporated several design elements to improve *in vivo* pharmacokinetics by bypassing RES mediated nanoparticle clearance mechanisms, the antibody fragmentation method utilized resulted in conjugation of non-functional fragments that reduced overall CD4 targeting specificity.[31]

In this work, we aimed to design hydrolytically degradable nanoparticles that specifically bind to CD4$^+$ helper T cell subsets to take advantage of their intrinsic lymphoid trafficking

abilities, while also overcoming their inability to perform professional phagocytosis, in order to target the delivery of hydrophobic eggmanone to the germinal centers of the spleen and lymph nodes. Furthermore, we wanted our base particle design to provide modular cargo encapsulation as well as the appropriate release kinetics to inhibit the differentiation of autoantibody producing plasma cells. We utilized two FDA-approved polymers, poly(lactic-co-glycolic acid) (PLGA) and polyethylene glycol (PEG), to generate hydrolytically degradable nanoparticles capable of providing tunable release rates and increased circulation half-life of eggmanone. Furthermore, we employed maleimide-thiol mediated conjugation of CD4 targeting F(ab') antibody fragments to enable sustained, local delivery of eggmanone on the surface of $CD4^+$ T cell membranes. To the best of our knowledge, this work represents the first characterization of immunomodulatory cargo delivery utilizing maleimide-thiol mediated conjugation of αCD4 F(ab') fragments to PEGylated PLGA nanoparticles

CHAPTER III

RESULTS AND DISCUSSION

Synthesis and Characterization of PEGylated PLGA Nanoparticles with Varied Cargo

Oil in water emulsion strategies were utilized to synthesize nanoparticles with various hydrophobic cargo (Figure 2 A), and maleimide-thiol click chemistry was utilized to decorate the surface of nanoparticles with targeting antibody fragments (Figure 2 B and C). In total, five nanoparticle formulations utilizing different molecular weight PLGA polymers (10 kDa and 25 kDa), different PLGA-PEG corona end-chemistries (Maleimide and Methyl), and different encapsulated cargo (blank, eggmanone, and DiD), were generated to evaluate the therapeutic potential of nanoparticle formulated eggmanone. Eggmanone[27] and fluorescent 1,1'-Dioctadecyl-3,3,3',3'-Tetramethylindodicarbocyanine, 4-Chlorobenzenesulfonate Salt (DiD[32]) were loaded into PEGylated PLGA nanoparticles in order to investigate whether eggmanone could be efficiently packaged and delivered to $CD4^+$ T cells.

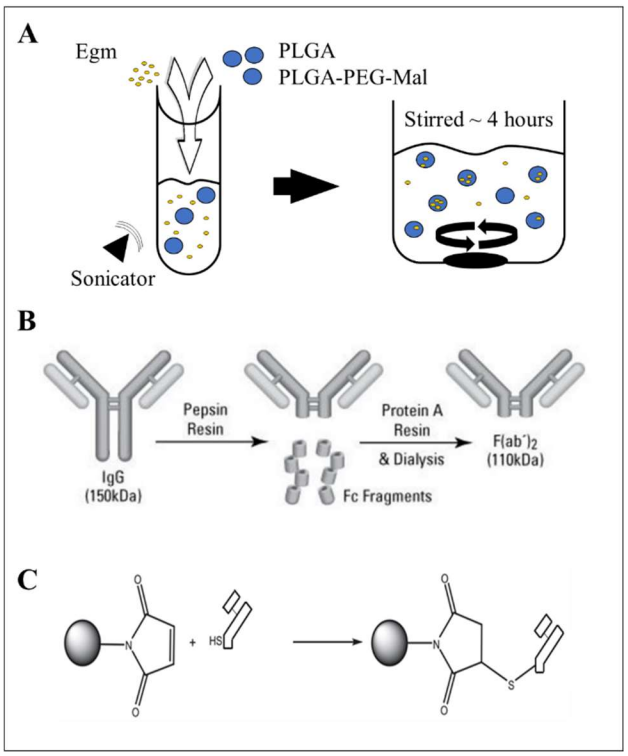

Figure 2: ***Particle Synthesis Strategy.*** **A)** Oil in water emulsions were created through sonication of PLGA(10 kDA)-PEG(5 kDa)-Maleimide or PLGA(10 kDA)-PEG(5 kDa)-Methyl, PLGA(10 kDa), and eggmanone dissolved in dichloromethane within an aqueous 0.25% polyvinyl alcohol surfactant solution. Dichloromethane was removed by evaporation facilitated by stirring of recovered emulsions. **B)** Targeting antibody fragments were generated through pepsin digestion. **C)** Antibody fragment disulfide bonds were reduced to expose thiol groups for conjugation to nanoparticles suspended in PBS via maleimide click chemistry. Figure adapted from.[33,34]

Importantly, loading of hydrophobic drugs such as eggmanone and/or DiD in formulations utilizing 10 kDa PLGA did not significantly affect particle size, polydispersity index (PDI) (Figure 3 A and B) or zeta potential (Figure 3 C) of synthesized nanoparticles as measured by dynamic and electrophoretic light scattering respectively. All formulations had zeta

potentials near -35 mV, sizes below 300 nm, and PDIs below 0.3. Therefore, particle suspensions were monodisperse, and of the appropriate size to provide passive accumulation in the spleen[35–37], in addition to T cell mediated transport to the spleen and lymph nodes.[38] Particle size, PDI, and zeta potential of formulations utilizing 25 kDa PLGA were also unaffected by encapsulation of cargo (Supplemental figure S1).

Zeta potential and particle size are both known to be important factors that influence the circulation half-life of nanoparticles, however, these factors were unaffected by cargo loading.[39] Additionally, the zeta potential of nanoparticle targeting systems has also been shown to dramatically affect the potential of nonspecific binding due to electrostatic interactions with the cell membrane. PLGA nanoparticles with cationic surface charges have been shown to preferentially interact with negatively charged cell membranes irrespective of targeting ligand conjugation[40]. Conversely, nanoparticles with anionic surface charges similar to our formulations have been shown to increase specific binding interaction to $CD4^+$ T cells by reducing nonspecific electrostatic interactions with cell membranes, and allowing conjugated targeting ligand binding affinity to dominate.[31] Therefore, we believe the measured zeta potentials of our undecorated: blank, eggmanone-loaded, and DiD-loaded nanoparticle formulations, to be ideal for antibody fragment mediated systemic targeting of $CD4^+$ T cells.

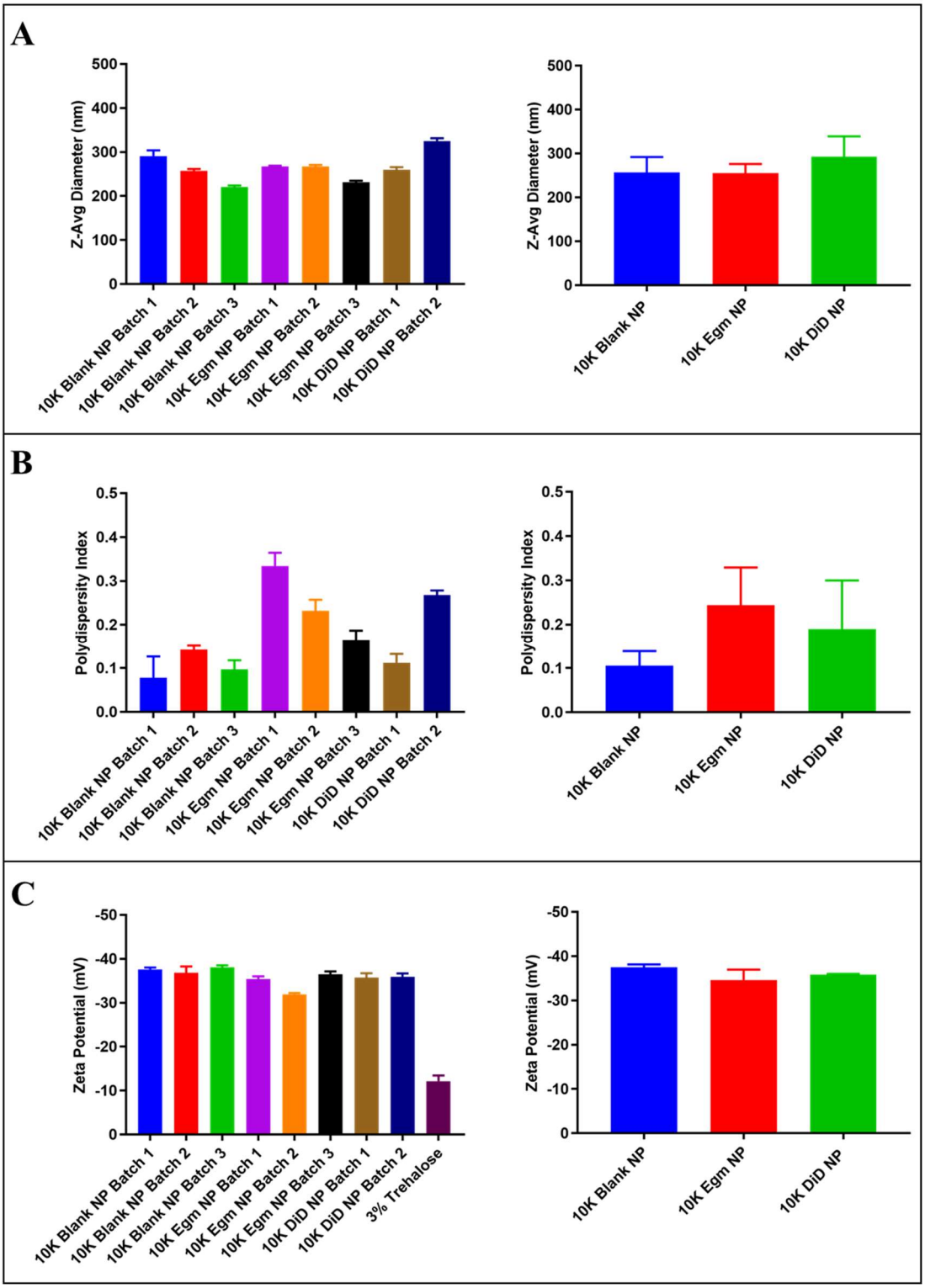

Figure 3: ***Undecorated 10 kDa Nanoparticle Physical Characterization.*** Dynamic light scattering measurements of eggmanone loaded, DiD loaded, and blank lyophilized nanoparticles

resuspended in DiH_2O revealed that all particle formulations were less than 300 nm in size **(A)**, monodisperse **(B)** and appropriately sized for targeting $CD4^+$ T cells in the blood and secondary lymphoid organs**.** Zeta potential measurements of the same nanoparticle suspensions and trehalose solution used for lyophilization procedures **(C)** were unaffected by particle loading and appropriate for antibody fragment mediated specific cell targeting. All nanoparticles were made with PLGA(10 kDa) and PLGA(10 kDa)-PEG(5 kDa)-Maleimide. No significant differences in average size, polydispersity index, or zeta potential were found using ordinary One-way ANOVA with Tukey's multiple comparisons test (n=3 batches for eggmanone loaded and blank nanoparticles and n=2 batches for DiD loaded nanoparticles).

We verified that the presence of maleimide reactive end-chemistry on PEGylated PLGA nanoparticle coronas was unaffected by eggmanone loading through 1H nuclear magnetic resonance spectroscopy of 10 kDa PLGA nanoparticle formulations made with either PLGA-PEG-Maleimide or PLGA-PEG-Methyl. NMR spectra of nanoparticles made with PLGA-PEG-Maleimide (Figure 4 B and C) all exhibited a peak at 6.7 ppm, characteristic of maleimide[41], that was not present in the spectra of particles made with PLGA-PEG-Methyl instead (Figure 4 A). Additionally, NMR spectra of nanoparticles loaded with eggmanone exhibited known characteristic peaks of eggmanone[42] (Figure 4 C) that, in addition to UV/VIS spectroscopy (approach shown in Supplemental Figure S2), confirmed the loading of eggmanone within nanoparticles at an encapsulation efficiency of $21.6 \pm 9.8\%$ (calculated from UV/VIS). Although encapsulation efficiencies above 50% are not uncommon for other PLGA nanoparticle formulations encapsulating unrelated hydrophobic agents, the use of lower molecular weight PLGA in our formulations may have resulted in reduced encapsulation efficiency. This could be

due to weaker hydrophobic interactions between eggmanone and the shorter hydrophobic regions of the low molecular weight PLGA polymer chains.[43] We chose to continue investigation of low molecular weight PLGA formulations, despite low encapsulation efficiency, in order to achieve the fastest release rates of eggmanone.[44] However, future studies will investigate the effects of PLGA molecular weight on eggmanone encapsulation efficiency. Additional NMR spectra of 25 kDa nanoparticles also revealed the presence of maleimide reactive end-chemistry in PEGylated PLGA nanoparticle coronas, but encapsulation efficiency for this formulation has not yet been determined (Supplemental Figure S3).

The release rate of eggmanone from nanoparticle formulations utilizing 10 kDa PLGA was investigated using fluorescent DiD as a surrogate compound for eggmanone due to insufficient limits of detection for eggmanone using UV/VIS spectroscopy. Nanoparticles incubated in PBS at 37 °C while shaking, released 74.5% of DiD over the course of 5 days, and exhibited a characteristic burst release associated with low molecular weight, 50:50 (lactic acid:glycolic acid) PLGA equal to 55.7% within the first 24 hours (Supplemental Figure S4). Although we did not directly measure the release of eggmanone from our formulation, we expect a similar and/or faster release profile since it is similarly hydrophobic and has a significantly lower molecular weight of 416 Da compared to 1052 Da for DiD. Moreover, the release kinetics we observed with DiD proved to be favorable for a therapeutic intervention strategy addressing the lag phase of a primary adaptive immune response to self-antigen. This period can be as short as 2-3 days or as long as several weeks. During this time, antigen presentation and subsequent isotype switching and differentiation of B cells into autoantibody-producing plasma cells, occurs in the germinal centers of secondary lymphoid organs. However, self-reactive antibodies are not produced until afterwards. Thus, if a sufficient number of eggmanone-loaded nanoparticles with

similar release kinetics could be targeted to the germinal centers during the lag phase, inhibition of plasma cell differentiation and autoantibody production could be achieved on a sufficient timescale to serve as a viable therapeutic intervention strategy for SLE.

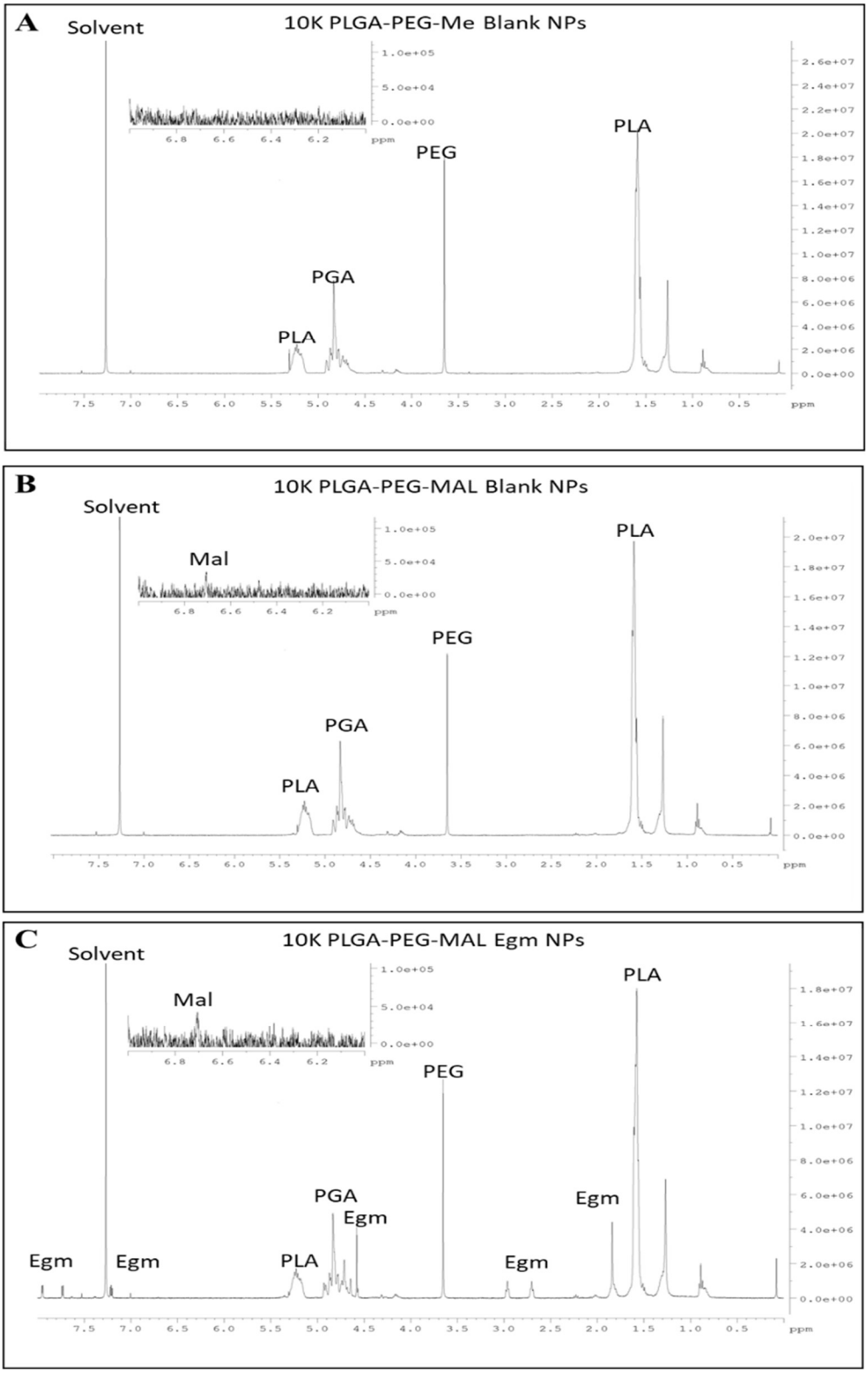

Figure 4: ***Undecorated 10 kDa Nanoparticle Chemical Characterization.*** NMR analysis of nanoparticles made with PLGA(10 kDa) and PLGA(10 kDa)-PEG(5 kDa)-Methyl **(A)**, compared

to nanoparticles made with PLGA(10 kDa)-PEG(5 kDa)-Maleimide **(B)**, confirms the presence of maleimide reactive end chemistry that was unaffected by eggmanone loading **(C)**. All particles were characterized using 1H nuclear magnetic resonance spectroscopy (Bruker, 400 MHz). All NMR were performed in deuterated chloroform. Abbreviations for analytes identified above include: eggmanone (Egm), poly(lactic acid) (PLA), poly(glycolic acid) (PGA), polyethylene glycol (PEG), maleimide (Mal).

Therapeutic Potential of Nanoparticle Formulated Eggmanone

After demonstrating that PEGylated PLGA nanoparticles could efficiently encapsulate and release eggmanone in a therapeutically relevant timeframe, we verified that nanoparticle formulation of eggmanone was as effective as the free drug at inhibiting antigen specific activation of $CD4^+$ T cells. Acute toxicity of eggmanone loaded and blank nanoparticle formulations was evaluated *ex vivo* 24 and 72 hours after incubation of resuspended nanoparticles with whole splenocyte cultures. No significant effects on the viability of splenocytes during 24-hour incubations were observed for formulations made with 25 kDa PLGA (Figure 5 A). However, formulations made with 10 kDa PLGA did exhibit acute particle toxicity up to 22% for eggmanone loaded and 17% for blank nanoparticles at particle concentrations equivalent to 10 μM eggmanone (Figure 5 B). Interestingly, no significant effects on viability were observed for particle concentrations equivalent to 1 μM eggmanone during 24-hour incubations, or either particle concentration during 72-hour incubations for formulations made with 10 kDa PLGA (Figure 5 B and C). Furthermore, *in vivo* administration of eggmanone-loaded nanoparticles will most likely result in equivalent eggmanone doses closer to

1 μM in the spleen due to distribution of nanoparticles in the blood and surrounding tissues following systemic administration.

Although 10 μM of eggmanone was administered for each formulation, the necessary concentration of resuspended lyophilizate needed for 10 kDa particles (0.227 mg/mL) was ~2.5 fold more concentrated than that used for 25 kDa (0.0867 mg/mL). The higher molecular weight of PLGA used in 25 kDa formulations could have increased encapsulation efficiency of eggmanone, resulting in higher eggmanone concentration per mg of lyophilizate. Therefore, the discrepancy in acute toxicity during 24-hour incubations could be due to increased polymer content administered to splenocyte cultures with 10 kDa particles. Future characterization of the encapsulation efficiency of 25 kDa batches will determine this. Furthermore, the discrepancy in cell viability for higher 10 kDa particle concentrations between 24 and 72 hours can be rationalized as follows. Although 10 kDa particles led to minor levels of acute particle toxicity at 24 hours, no artificial stimulation signals were provided during these experiments, which could have caused cell death of primary lymphocytes that require stimulation of the TCR, BCR and costimulatory receptors to remain viable for extended periods of time. Therefore, over the 72-hour incubation period, the lack of artificial stimulation in splenocyte cultures could have caused an independent cell death event large enough to mask the contribution of acute nanoparticle toxicity.

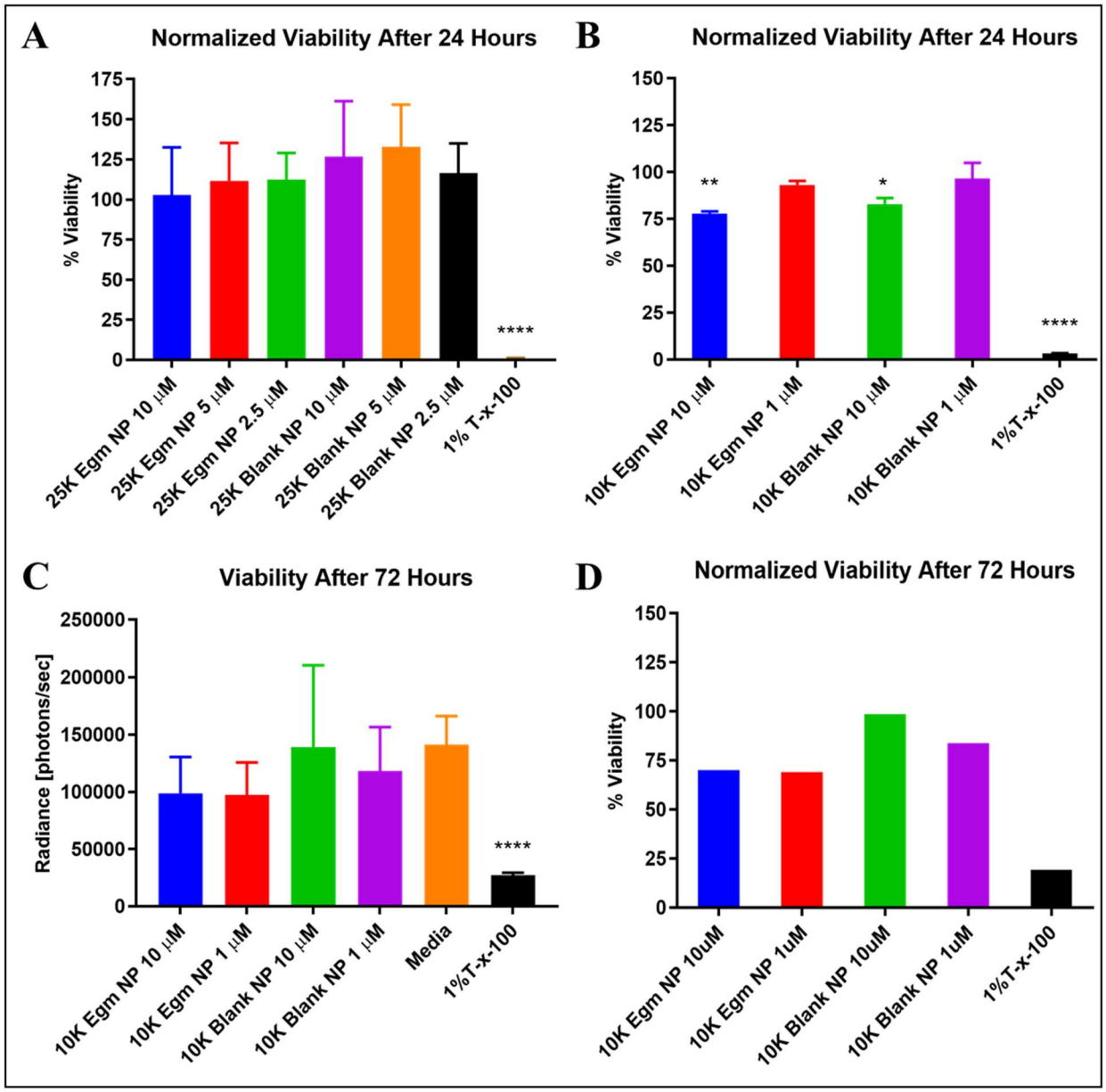

Figure 5: ***Ex Vivo Evaluation of Nanoparticle Biocompatibility.*** Average viability normalized to media controls of whole splenocytes incubated for 24 hours with eggmanone loaded and blank particles made with 25 kDa (n=3 spleens) **(A)**, and 10 kDa (n=2 spleens) PLGA **(B)** revealed that only high concentrations of 10 kDa particles demonstrated acute toxicities. Viability of whole splenocytes incubated for 72 hours with eggmanone loaded and blank particles made with 10 kDa PLGA **(C)**, and average viability normalized to media of technical replicates (n=1 spleen) for the same experiment revealed no significant differences in toxicity **(D)**. Final eggmanone

concentration of particle suspension listed with matched blank particle concentrations. Viability was evaluated using CellTiter Glo assay measured by IVIS with 1% triton-x-100 (1% T-x-100) as a positive cell death control. Whole splenocytes were derived from female FVB mice. (*$p<0.05$, **$p<0.005$, ****$p<0.0001$ for ordinary One-way ANOVA with Dunnett's multiple comparisons test were performed for each nanoparticle formulation compared to media controls at each concentration listed).

The FVB mice used for viability experiments do possess any model antigen specificity, unlike transgenic OT-II mice that express $CD4^+$ T cell TCRs specific for ovalbumin. *Ex vivo* stimulation of OT-II splenocytes with ovalbumin and subsequent evaluation of inflammatory cytokine production can, therefore, be used as a high throughput model of antigen specific autoimmunity. IFN-γ is the hallmark cytokine produced by $CD4^+$ T follicular helper cells (Tfh) in the germinal center response that enables B cell production of high affinity, long circulating IgG antibody isotypes.[45] Inhibition of interferon gamma (IFN-γ) production by OT-II splenocytes stimulated with ovalbumin was measured 72 hours after incubation with eggmanone loaded or blank, undecorated nanoparticle formulations made with 25 kDa PLGA. For all concentrations of eggmanone evaluated, both free and nanoparticle formulations of eggmanone significantly inhibited the production of IFN-γ compared to media controls. No significant changes were observed for DMSO and blank nanoparticle vehicle controls (Figure 6). Additionally, the lack of any IFN-γ inhibition after treatment with blank nanoparticles is further evidence that the 25 kDa formulation is also nontoxic at longer timepoints.

In combination with the lack of acute toxicity observed for 25 kDa formulations (Figure 5 A and Figure 6), characterization of nanoparticle release rate (Supplemental Figure S4), and

ovalbumin antigen specificity associated with OT-II $CD4^+$ T cells, IFN-γ inhibition during 72-hour incubations was inferred to be the result of efficient release of eggmanone from nanoparticles that inhibited the activation of $CD4^+$ T cells undergoing antigen presentation. However, at this time it is unclear if the inhibition is due to eggmanone delivery to $CD4^+$ T cells or antigen presenting cells in the surrounding culture. Future experiments utilizing CD4-targeted, eggmanone-loaded nanoparticles will directly measure the contribution of targeted eggmanone to either cell type. Nevertheless, we have demonstrated the first characterization of antigen specific $CD4^+$ T cell inhibition mediated by nanoparticle formulated eggmanone delivery.

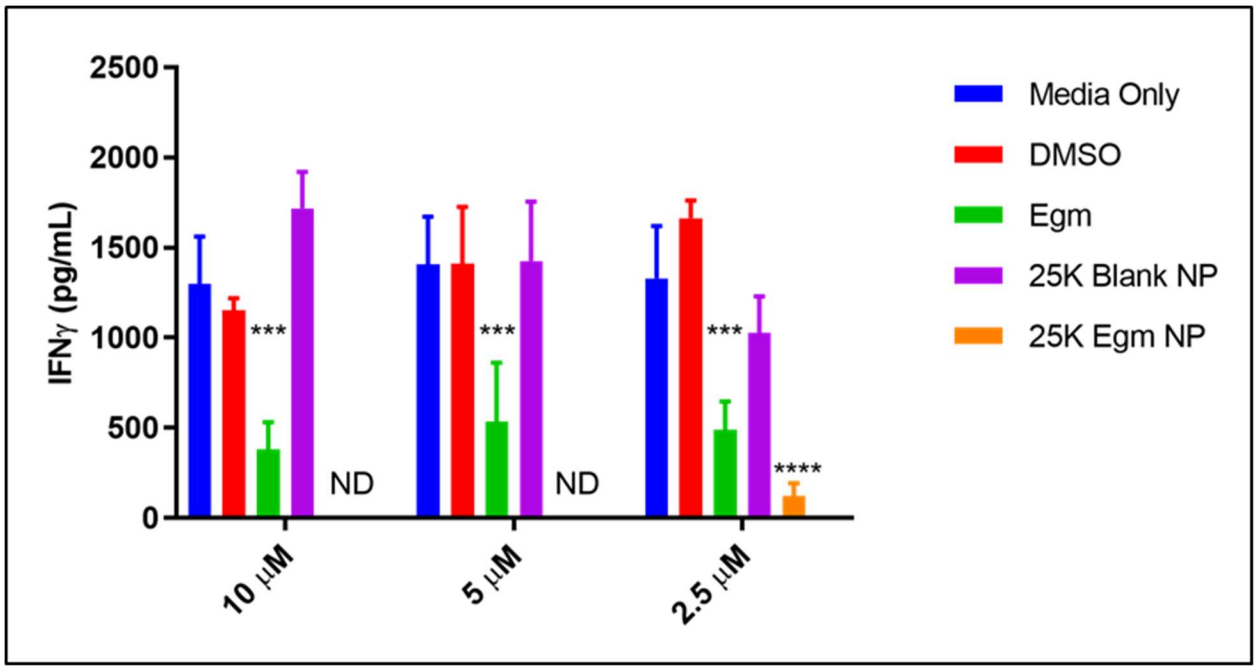

Figure 6: ***Ex vivo Inhibition of T cell Activation with Undecorated 25 kDa Nanoparticles.*** Interferon gamma (IFN-γ) production measured by ELISA from OT-II splenocytes stimulated with 50 μg/mL whole ovalbumin and incubated with vehicle controls, eggmanone in DMSO, and eggmanone loaded nanoparticles for 72 hours. Both free eggmanone and eggmanone-loaded

particles significantly inhibited IFN-γ production compared to media controls. No significant effects were observed for DMSO and blank particle vehicle controls. Nanoparticles were made with 25 kDa PLGA and eggmanone concentration of particle suspensions was measured by UV/VIS. Particle concentrations of blank particle suspensions (no eggmanone) were matched to equivalent eggmanone loaded particle concentrations. Data representative of 2 experiments. Whole splenocyte cultures were derived from female OT-II mice. (n=1 spleen, ***$p<0.0005$, ****$p<0.0001$, ordinary Two-way ANOVA with Dunnett's multiple comparisons test were performed for each nanoparticle formulation compared to media controls at each concentration listed).

Anti-CD4 Antibody Decoration and Evaluation of Targeting Specificity

Successful encapsulation of fluorescent DiD within 10 kDa PEGylated PLGA nanoparticles enabled the characterization of $CD4^+$ T cell targeting specificity afforded by maleimide-thiol antibody fragment decoration. α-CD4 and isotype control F(ab') antibody fragments were conjugated to the surface of 10 kDa DiD-loaded nanoparticles (DiD-NP) and incubated for 30 minutes with whole splenocyte cultures derived from immunocompetent mice. Evaluation of DiD^+, nanoparticle bound immune cell subtypes was performed via flow cytometry (Figure 7 A and B).

Of the total number of cells incubated with α-CD4 decorated particles that were DiD^+, ~75% were $CD4^+$ T cells, ~13% were B cells, ~8% were non-T, non-B cells, and ~ 4% were $CD8^+$ T cells (representative results obtained from the experiment summarized in Figure 7 A and B). Given this result, we analyzed $DiD^+/CD4^+$ T cells, $CD8^+$ T cells, and non-T cells (B cells, dendritic cells, and macrophages) to determine nanoparticle CD4 targeting specificity. α-CD4 decorated particles achieved ~ 88% $CD4^+$ T cell staining, and significantly increased targeting specificity for $CD4^+$ T cells compared to isotype (~6%) and undecorated controls (~2%). Additionally, α-CD4 decorated particles also targeted $CD4^+$ T cells significantly more than $CD8^+$ T cells (~11%) and non-T cells (~10%) (Figure 7 C). In all cases, undecorated and untargeted isotype-decorated particles exhibited low levels of nonspecific binding that was presumably due to electrostatic repulsion of negatively charged cell membranes mediated by sufficiently negative zeta potentials achieved in our formulations (Figure 3 C). Therefore, the high degree of targeting specificity achieved by α-CD4 decorated particles was almost certainly due to zeta potential mediated electrostatic repulsion from nonspecific cell types that was overcome by antibody fragment affinity for $CD4^+$ T cells.

Collectively, our results demonstrated that the nanoparticle formulation designed and fabricated in this study yielded low levels of non-specific binding, and superior levels of CD4 targeting specificity than previously published competing particle designs.[31] More importantly, we were able to achieve these results in a physiologically relevant heterogenous whole splenocyte population, rather than purified T cell populations.[38] Although we did not directly measure the efficiency of antibody fragment decoration of our formulations, the high levels of $CD4^+$ T cells targeting specificity that we achieved *ex vivo* prompted us to evaluate the same measurements *in vivo* following systemic administration.

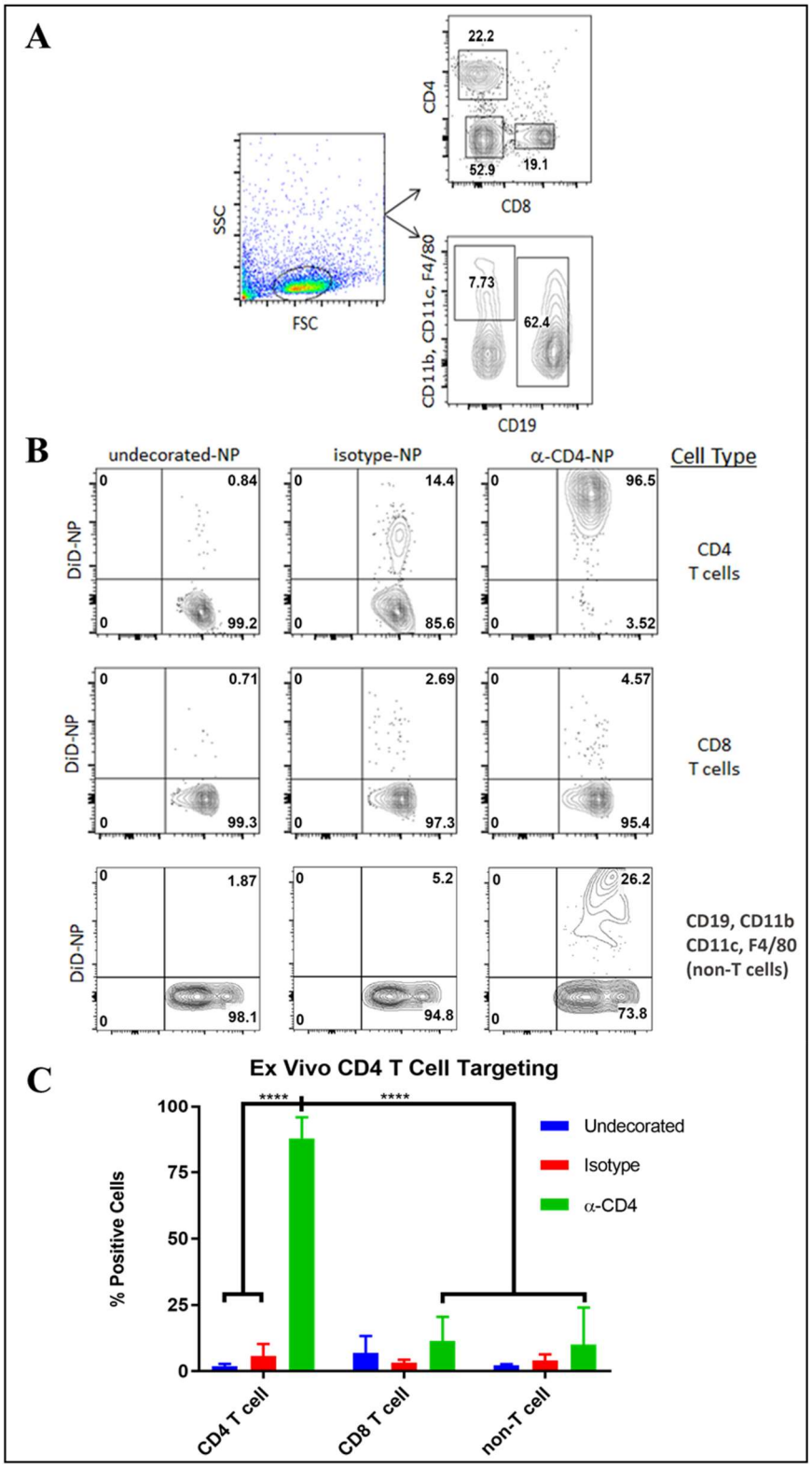

Figure 7: ***Ex Vivo CD4 T cell Targeting.*** Flow cytometry gating strategy used to analyze the targeting specificity of α-CD4 decorated, DiD-loaded fluorescent nanoparticles (DiD-NP) **(A)**,

and representative staining results of 3 experiments **(B)**, revealed increased affinity of α-CD4 decorated particles for CD4 T cells and low levels of nonspecific binding among all cell types investigated. The x-axis of nanoparticle plots corresponds to the cell type displayed on the far right. Quantification of DiD positive splenocytes incubated for 30 minutes with either undecorated, isotype control decorated, or α-CD4 decorated fluorescent nanoparticles suspended in PBS **(C)** revealed significantly increased CD4 targeting specificity of α-CD4 decorated particles. Flow cytometry probe for CD4 staining utilized a an antibody clone that recognized a different epitope of CD4 than those used to decorate nanoparticles. Nanoparticles were made with PLGA(10 kDa) and PLGA(10 kDa)-PEG(5 kDa)-Maleimide. Splenocytes were derived from female C57BL/6J mice. (n=3 spleens, ****$p < 0.0001$, ordinary Two-way ANOVA with Tukey's multiple comparisons tests were performed for each particle formulation within a given cell population and also across each cell population for a given particle formulation).

After successfully achieving *ex vivo* $CD4^+$ T cell targeting specificity, we then evaluated the *in vivo* capabilities of the same nanoparticle formulation in immunocompetent mice. DiD-loaded nanoparticles were decorated with either α-CD4 or isotype control antibody fragments and retro-orbitally injected into female C57BL/6J mice. 18 hours after administration, the spleen, inguinal lymph nodes, and liver, were collected for evaluation of nanoparticle biodistribution and targeting specificity among various immune cell subsets. No detectable DiD signal was observed in the lymph nodes, and we believe this to be due to the lack of a draining lymph node following systemic administration. Nanoparticles injected into the retro-orbital sinus drain directly into the jugular vein before reaching the heart and entering the arterial bloodstream. At this time, CD4 targeted nanoparticles bind the CD4 surface receptors of naïve T cells circulating in the blood

before they enter secondary lymphoid organs to undergo antigen presentation, activation, and initiation of germinal center responses. Consequentially, there is no way to predict which lymph node nanoparticle bound $CD4^+$ T cells will traffic to as there is in other experimental models utilizing tumor draining lymph nodes.[38] Future experiments utilizing adoptively transferred, nanoparticle bound $CD4^+$ T cells, will evaluate their lymph node homing potential.

Similar to the observation resulting from experiments utilizing *ex vivo* splenocyte cultures, α-CD4 decorated particles achieved ~ 21% $CD4^+$ T cell staining in the spleen, and significantly increased targeting specificity for $CD4^+$ T cells compared to isotype (~7%) controls. Additionally, targeting of $CD4^+$ T cells by α-CD4 decorated particles in the spleen was confirmed by significantly elevated staining levels compared to $CD8^+$ T cells (~8%) and non-T cells (~6%) (Figure 8 A). No statistical differences in staining levels were observed for isotype control decorated particles, confirming that binding was the result of non-specific interactions. CD4 targeting specificity was not conserved in the liver, a known biological sequestration site of nanoparticle therapeutics, where antibody fragment decoration had no effect on targeting specificity, and the majority of particles were bound to non-T cells (~15%) (Figure 8 B). Macrophage populations in the liver often nonspecifically uptake nanoparticles < 500 nm in diameter over a wide range of formulations, and nanoparticles greater than 250 nm will often accumulate in the liver after systemic administration.[35,36,46,47] Therefore, the majority of DiD-loaded nanoparticles in the liver were accumulated by non-T cell populations due to non-specific uptake by macrophages. Despite this, CD4 targeting specificity levels for α-CD4 decorated particles were higher in the spleen compared to isotype and α-CD4 decorated particles in the liver. These results suggest that the intrinsic lymphatic trafficking abilities of helper T cells

circulating in the blood may provide preferential accumulation of α-CD4 decorated nanoparticles in the spleen that can be leveraged for therapeutic inhibition of germinal center responses.

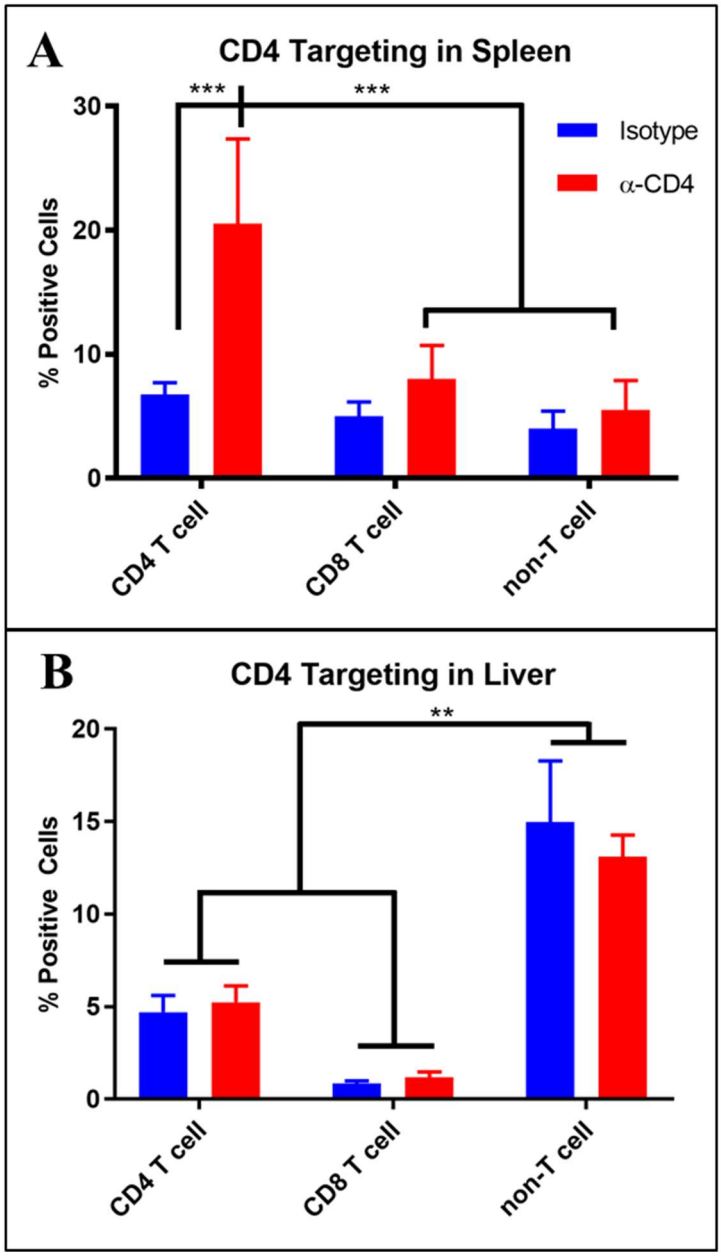

Figure 8: ***In Vivo CD4 T cell Targeting.*** Quantification of DiD positive immune cells (gating strategy shown in **Fig 4**) isolated from the spleen **(A)**, and liver **(B)** 18 hours after retro-orbital

injection of 2 mg of either isotype control decorated, or α-CD4 decorated fluorescent nanoparticles suspended in PBS. Mass of nanoparticles injected was equal to the mass of lyophilizate including trehalose suspended in a 200 μL injection volume. Significant increases in CD4 targeting specificity in the spleen achieved by α-CD4 decorated particles compared to isotype control decorated particles were not conserved in the liver. Nanoparticles were made with PLGA(10 kDa) and PLGA(10 kDa)-PEG(5 kDa)-Maleimide (n=4 mice, **$p < 0.005$ and *** $p = 0.0001$, ordinary Two-way ANOVA with Tukey's multiple comparisons tests were performed for each particle formulation within a given cell population and also across each cell population for a given particle formulation).

CHAPTER IV

CONCLUSIONS AND FUTURE WORK

In this work, we synthesized and characterized 5 PEGylated PLGA nanoparticle formulations for specific delivery of hydrophobic small molecule drugs to $CD4^+$ T cells. Our results demonstrated that encapsulation of eggmanone did not affect the physical or chemical characteristics important for *in vivo* administration and cell-targeted delivery of cargo. We verified that nanoparticle formulations of eggmanone made from the FDA approved polymers PLGA and PEG were biocompatible and capable of releasing the majority of their payload in a therapeutically relevant timeframe. Using maleimide-thiol "click" chemistry conjugation of targeting antibody fragments, we were able to achieve high levels of $CD4^+$ T cell targeting specificity *ex vivo* and *in vivo*, with a minimal degree of non-specific particle uptake. Furthermore, we have demonstrated antigen specific inhibition of $CD4^+$ T cell activation mediated by nanoparticle formulated eggmanone. Collectively, this work represents the research and development of a rationally designed nanoparticle delivery vehicle capable of systemic administration of hydrophobic immunomodulatory drugs for the treatment of T cell hyperactivity in autoimmunity.

Although we limited the investigation of our formulation to $CD4^+$ T cells, another group has recently validated a similar formulation for delivery to $CD8^+$ T cells.[38] In fact, the conjugation mechanism of our formulation could presumably enable specific delivery of hydrophobic cargo to a variety of immune cells simply by substituting the targeting antibody fragments that decorate the surface of synthesized particles. We highlighted the clinical potential of eggmanone delivery for the treatment of SLE, however, our formulation is broadly applicable

for a variety of autoimmune rheumatic diseases such as: rheumatoid arthritis, scleroderma, and autoimmune myositis. Additionally, numerous FDA approved hydrophobic immunosuppressants are currently used to broadly suppress the immune systems of patients with autoimmune diseases so that disease symptoms can be managed. The modular encapsulation mechanism employed by our formulation could enable specific delivery of these agents and improve therapeutic administration by limiting the necessary dosage, reducing off-target toxicities, and mitigating opportunistic infection.

Future experiments will focus on characterizing nanoparticle biodistribution over time following intravenous administration, to determine optimal therapeutic administration strategies. Optimization of the current formulation components will be performed to achieve the highest circulation half-life, encapsulation efficiency, and biocompatibility of nanoparticle formulated eggmanone. Additionally, experiments utilizing prophylactic and therapeutic administration of CD4 targeted, nanoparticle formulated eggmanone still need to be performed in order to elucidate the potential of Hh signaling inhibition for the restoration of peripheral tolerance mechanisms that are deficient in SLE.

CHAPTER V

MATERIALS AND METHODS

Materials

Flow Cytometry Staining Probes

Product information for the fluorescently labeled antibodies used in the flow cytometry staining protocols within this work are provided in the following format: (surface marker-color, company, product #, final dilution). Flow cytometry staining probes used consisted of: (TCRBeta-FITC, BD-Pharmigen, 553171, 1:200), (CD4-Percp-Cy5, Biolegend, 116012, 1:300), (CD19-PECy7, BD Pharmigen, 552854, 1:200), (CD8-APCCy7, Tonbo, 25-0081-0100, 1:200), (CD11C-FITC, Tonbo, 35-0114-U100, 1:200), (CD11B- PE, Tonbo, 50-0112-U100, 1: 300), (F480-PECY7, ebioscience, 25-4801-82, 1: 200), and (B220-APCCY7, Tonbo, 25-0452-U100, 1: 200).

Methods

Nanoparticle formulation

PEGylated PLGA nanoparticles were prepared using oil in water emulsion mediated by sonication. PLGA 50:50 LA:GA(10 kDa)-PEG(5 kDa)-Maleimide (Nanosoft Polymers, lot number 27910051517) or PLGA 50:50 LA:GA(10 kDa)-PEG(5 kDa)-Methyl (Nanosoft Polymers, lot number 275310050324) was added to PLGA 50:50 LA:GA (10 kDa, Durect corporation, lot number 902-82-1 and/or 25 kDa Sigma lot number MKCC6770) at 25% (wt PLGA-PEG/wt PLGA) and dissolved in dichloromethane at 2% (wt polymer/v DCM). Hydrophobic eggmanone and/or DiD cargo was incorporated into the oil phase prior to

sonication for encapsulation within PLGA-PEG nanoparticles. Eggmanone powder was dissolved directly in DCM 25% (wt eggmanone/wt total polymer) prior to polymer while 2 uL (for in vitro targeting experiments) and 10 uL (for in vivo targeting experiments) of DiD dissolved in DMSO at 2mg/mL was added after polymers were fully dissolved. Resulting solutions were transferred to ice-cold 0.25% (w/v) poly-vinyl-alcohol in deionized water surfactant solution. Emulsification was achieved using a Fisher Scientific Sonic Dismembrator (Power level 3, 3 x 10 second on/off cycles on ice). The resulting nanoparticle suspension was stirred for 4 hours to both remove residual dichloromethane, and allow nanoparticles to harden, before they were washed with PBS via centrifugation (20,000 G, 10 min) to remove residual poly-vinyl-alcohol. Recovered nanoparticles were suspended in either PBS (for chemical analysis) or 3% trehalose (Sigma) and filtered with 5 μm (Pall, acrodisc supor membrane) followed by 0.45 μm (ThermoFisher PTFE) syringe filters prior to lyophilization (-40 C, 0.2 mbar).

Characterization of eggmanone-loaded nanoparticle encapsulation efficiency

Absorbance spectra of eggmanone and PLGA in DMSO were measured in both quartz and disposable polystyrene cuvettes to evaluate spectral overlap at the 323 nm wavelength. Eggmanone and eggmanone-loaded nanoparticle lyophilizate without trehalose was dissolved in dimethyl sulfoxide for evaluation of peak eggmanone absorbance at 323 nm by UV/VIS spectroscopy. At least three technical replicates of 180 uL volumes were prepared for each sample. Measurements were performed in UV-transparent 96-well plates (Nunc, 96-well UV microplates) using a Biotek M1000Pro plate reader. Measured eggmanone-loaded nanoparticle absorbance values were adjusted to remove the contribution of PLGA by subtracting absorbance values of matched concentration unloaded particles. Encapsulation efficiency was calculated as

the ratio of experimental loading capacity determined by UV/VIS spectroscopy to theoretical loading capacity.

Characterization of nanoparticle size, zeta potential, reactive chemistry, and release rate

Nanoparticle size and zeta potential were measured using dynamic light scattering (Malvern Zetasizer Nano ZS). Nanoparticle lyophilizate was resuspended in deionized water at a final concentration of 0.5 mg/mL for these measurements. The suspension was homogenized through vortex mixing and aggregates dispersed removed using a water bath sonicator (Cole-Palmer, Ultrasonic). Maleimide reactive end chemistry was verified using 1H nuclear magnetic resonance spectroscopy (Bruker, 400MHz). At least 5mg of nanoparticle lyophilizate without trehalose was dissolved in 600 uL deuterated chloroform (Sigma) in 1 dram glass vials for NMR sample preparation. Each sample was sealed with parafilm and vortex mixed until the sample was fully dissolved before loading into NMR tubes (Wilmad Precision) with a 1mL syringe. DiD release rate was measured using a Biotek M1000Pro plate reader. Nanoparticle lyophilizate was resuspended in 1XPBS and incubated at 37 °C while shaking for up to 5 days. Release times were staggered so that all samples were collected at once. Following incubation, nanoparticles were centrifuged (20,000 G, 10 min), and supernatant was decanted. Remaining DiD was quantified after suspending collected pellets in DMSO, and amount released was quantified by comparing DiD fluorescence of incubated particles to a 0 hr control.

Antibody conjugation to nanoparticles

αCD4 (clone GK1.5, Bio X Cell) and isotype control (clone LTF-2, Bio X Cell) $F(ab')_2$ antibody fragments were generated using the Pierce Fab Prep kit. Disulfide bonds between antibody fragments were reduced using 0.5 mM DTT in 1XPBS for 30 minutes at room temperature. Excess DTT was removed from fragments using 7K MWCO zebra spin filters

(ThermoFisher). Reduced antibody fragment concentration was quantified using nanodrop (Mettler Toledo UV5 nano) as recommended by ThermoFisher (280 nm absorbance, molar extinction coefficient = 1.4). Fragments were added to resuspended nanoparticles at a concentration of 25 ug antibody per 1 mg resuspended nanoparticle lyophilizate containing trehalose in 1X PBS (calcium and magnesium free). Resulting solutions were prepared with a final volume of 1 mL and shaken for 2 hours in 2 mL microcentrifuge tubes at room temperature on a Fisher mini vortexer (speed 8) to initiate Maleimide-thiol antibody conjugation to nanoparticles. Antibody conjugated particle solutions were used immediately after conjugation was complete.

Cell culture

Whole splenocyte cultures were derived from spleens harvested from 8-10-week-old female FVB mice (for evaluation of nanoparticle toxicity), C57BL/6J mice (for evaluation of nanoparticle targeting specificity), and OT-II mice (for evaluation of therapeutic efficacy). Mice were euthanized and spleens were immediately harvested and placed in ice-cold T cell media (RPMI-1640 supplemented with 10-20% FCS, pen/strep, 55 mM 2-mercaptoethanol, 1mM pyruvate, 2mM glutamine and non-essential amino acids). Spleens were manually dissociated using 40-micron cell strainers (Fisher Scientific, nylon mesh) and the resulting cell suspension was centrifuged at 1500 rpm for 7 min at 4 degrees Celsius. Supernatant was decanted and residual cell pellets were broken up. Red blood cells in the resulting cell suspension were lysed by adding 900 uL of microbiology grade water (Corning) followed by 100uL of 10X PBS (Sigma) while vortex mixing.

Evaluation of eggmanone-loaded nanoparticle therapeutic efficacy and biocompatibility

Whole splenocytes were seeded in standard (for evaluation of therapeutic efficacy) or black-walled (for evaluation of biocompatibility) 96-well plates at 100K cells/well for 24 hours prior to adding nanoparticle treatments. Eggmanone loaded and unloaded nanoparticle lyophilizate was resuspended in T cell media (mentioned above) via vortex mixing and water bath sonication immediately prior to use. Standard media was replaced with nanoparticle containing media, and cell viability was evaluated 24 and 72 hours later via Celltiter glo assay (Promega). IFN-γ production was evaluated 72 hours after stimulation with 50 μg/mL ovalbumin and nanoparticles via ELISA.

Evaluation of antibody-conjugated nanoparticle targeting efficacy

Targeting efficacy was evaluated using DiD (Invitrogen, D7757)-loaded antibody-conjugated fluorescent nanoparticles. *Ex vivo* targeting efficacy was evaluated in whole splenocyte cultures after a 30-minute incubation of DiD-loaded, antibody fragment decorated nanoparticles suspended in PBS via flow cytometry (250K cells/25 μg lyophilizate). *In vivo* targeting efficacy was evaluated in female C57BL/6J mice through retro-orbital injections of 200 μL DiD-loaded, antibody fragment decorated nanoparticles suspended in PBS (10 mg/mL lyophilizate). 18 hours after injection, the spleen, liver, and lymph nodes were collected for investigation of particle targeting efficacy via flow cytometry.

Flow cytometry

Cells were incubated with Fc block at 1:100 for 15 minutes at room temp in FACS buffer containing HBSS, 1% BSA, 4.17 mM sodium bicarbonate, and 3.08 mM sodium azide. Cells were labeled with an antibody cocktail consisting of either (TCRβ-FITC 1:200, CD4-Percp-Cy5 1:300, CD19-PECy7 1:200, CD8-APCCy7 1:200) or (CD11C-FITC 1:200, CD11B-PE 1:300, F4/80-PECY7 1:200, CD4-Percp-Cy5 1:300, B220-APCCy7 1:200) in FACS buffer for 30

minutes on ice in the dark. Cells were washed and resuspended in 2% PFA for analysis on a MACSQuant seven-color flow cytometer (Miltenyi Biotec), and data were analyzed using FlowJo Single Cell Analysis Version 10.0.1.

Animal experiments

All animal experiments were conducted in accordance with the Vanderbilt Institutional Animal Care and Use Committee. 8-10 week old female mice (FVB (FVB/NJ stock no: 001800), C57BL/6J stock no: 000664, and OT-II (B6.Cg-Tg(TcraTcrb)425Cbn/J stock no: 004194),The Jackson Laboratory) were used for all experiments.

Statistical Analysis

All error bars presented represent standard deviation unless otherwise indicated. One or Two-way Analysis of Variance followed by multiple comparisons test were performed for most data presented here, and statistical significance was defined as $p < 0.05$. Statistical analyses were performed using Prism 7.0 (GraphPad Software).

APPENDIX

SUPPLEMENTAL FIGURES

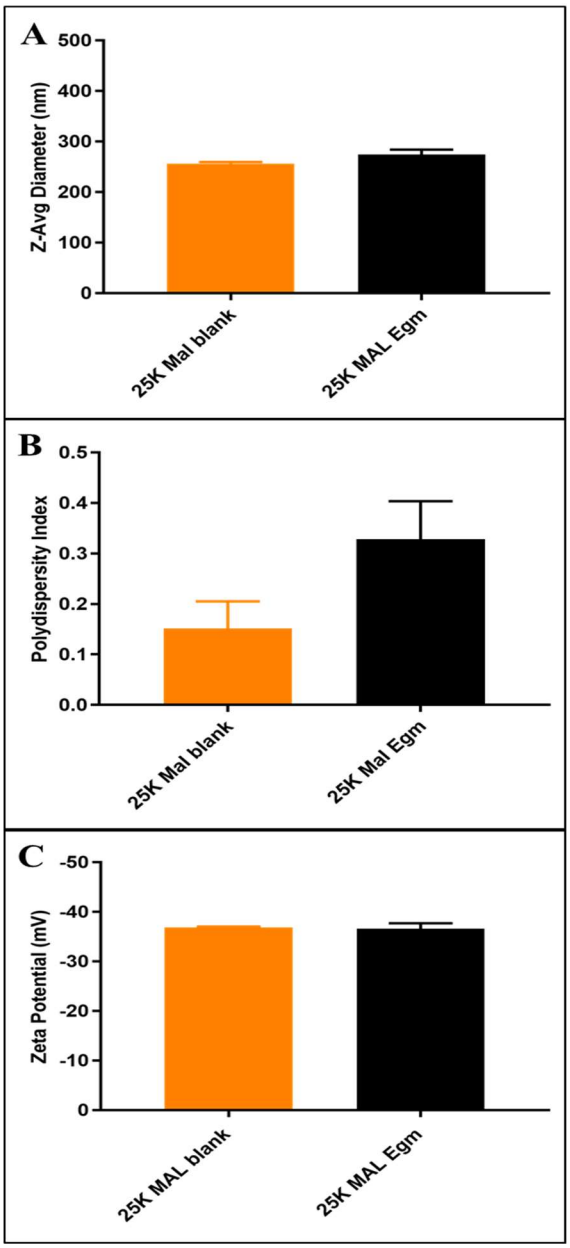

Supplemental Figure S1. Undecorated 25 kDa Nanoparticle Physical Characterization. **A and B)** Dynamic light scattering of eggmanone loaded and blank nanoparticles made with 25kDa

PLGA (n=1). **C)** Zeta potential measurements of the same nanoparticle formulations. Error bars represent technical replicate measures of n=1 batch for each formulation.

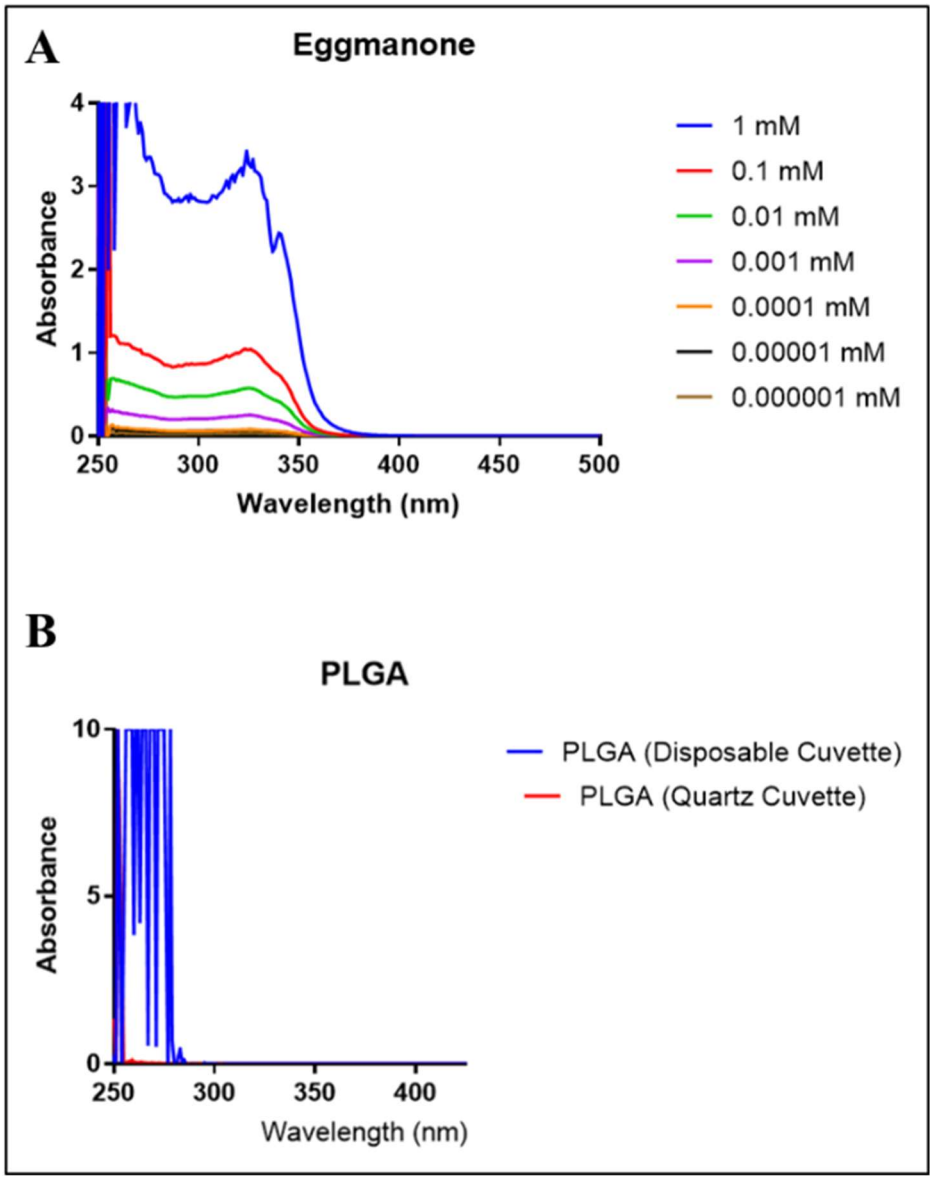

Supplemental Figure S2. UV/VIS Analysis of Eggmanone Absorbance Maximum. **A)** Absorbance spectra of eggmanone solutions prepared in DMSO measured in UV-transparent quartz cuvettes. An absorbance maximum for eggmanone was observed at 323 nm and the

effective detection range was found to be between 1 mM and 0.0001 mM for encapsulation efficiency measures. **B)** Absorbance spectra of PLGA solutions in DMSO in disposable polystyrene or quartz cuvettes. PLGA did not demonstrate significant absorbance at 323 nm when using UV-transparent cuvettes.

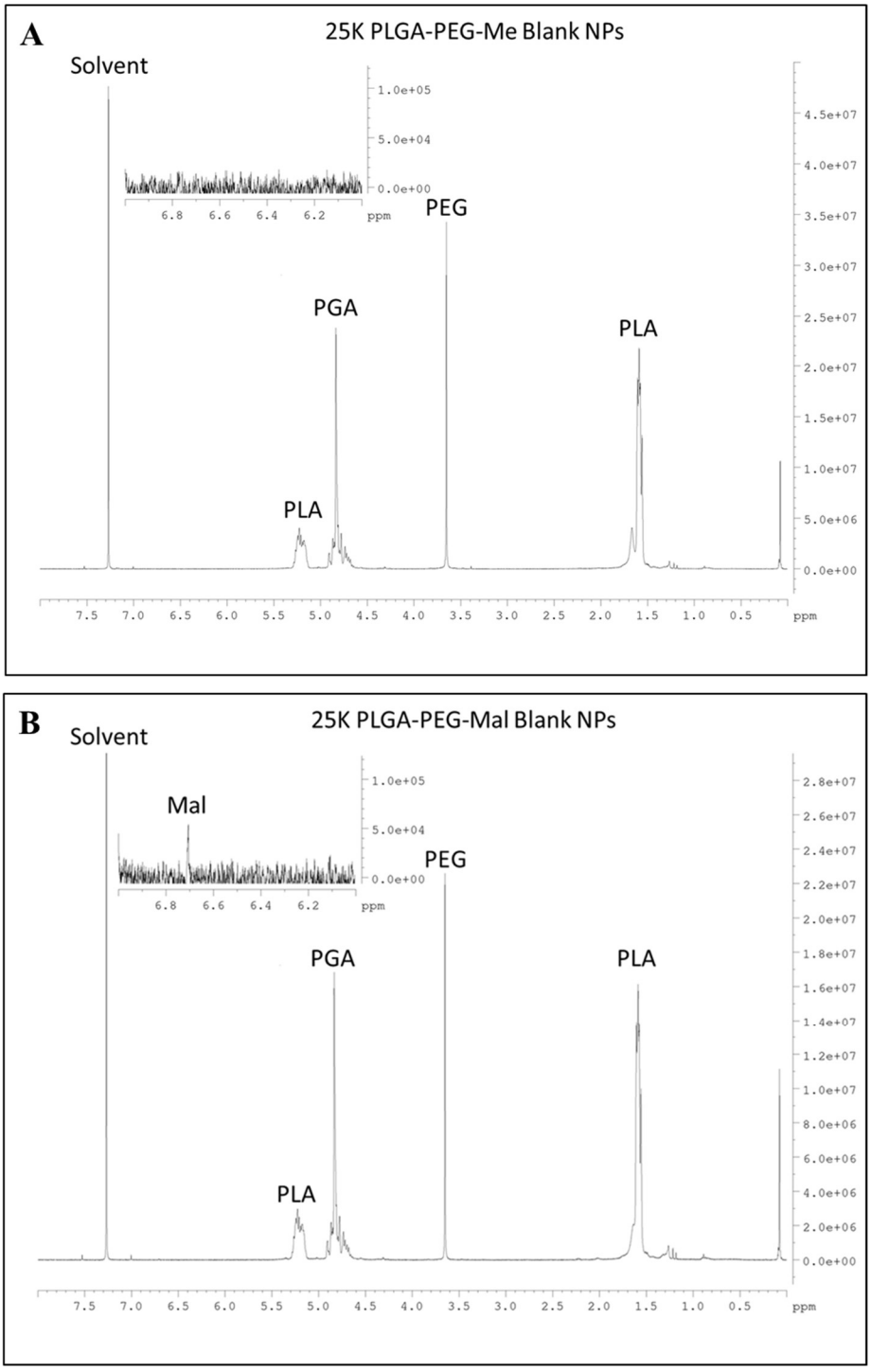

Supplemental Figure S3. Undecorated 25 kDa Nanoparticle Chemical Characterization. **A)** NMR spectra of synthesized nanoparticles made with 25 kDa PLGA and PLGA-PEG-Methyl or **B)** PLGA-PEG-maleimide.

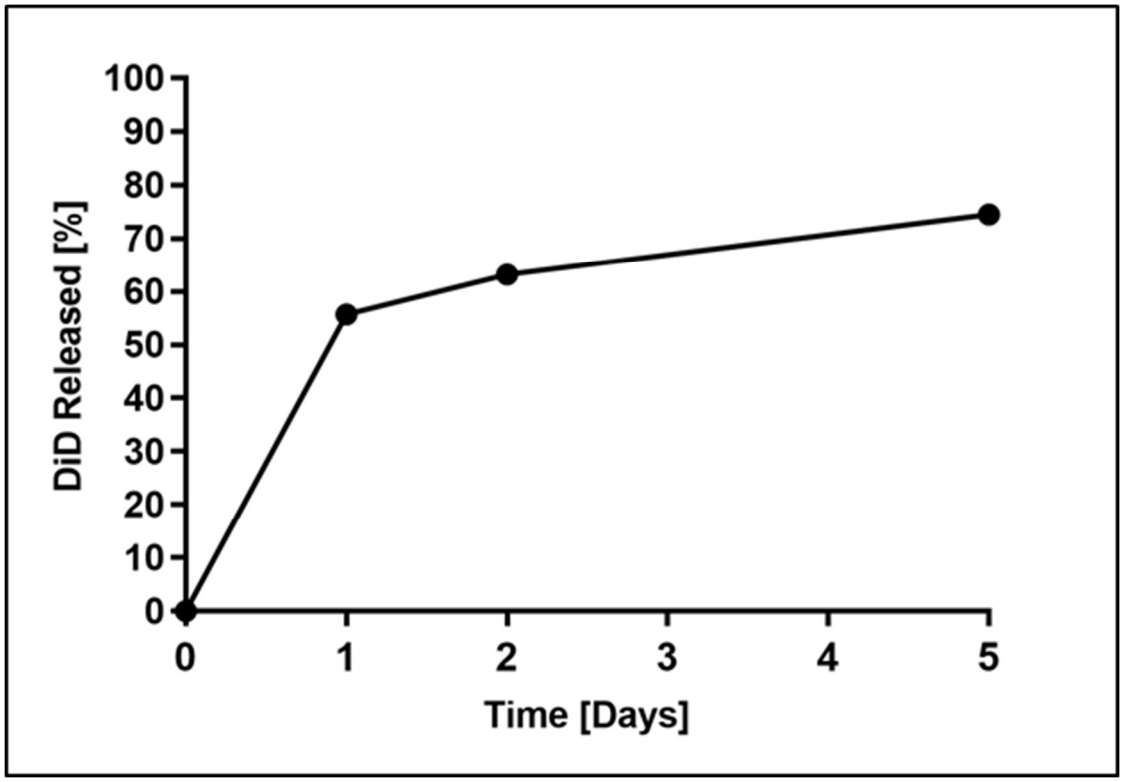

Supplemental Figure S4. 10 kDa Nanoparticle Release of DiD. Cumulative release profile of fluorescent DiD from nanoparticle suspensions made with 10 kDa PLGA incubated in PBS at 37C (n=1). Nearly 60% of DiD was released from DiD loaded nanoparticles during the initial 24 hour burst release period. After a period of 5 days, nearly 75% of DiD was released from loaded nanoparticles. Release values were calculated by normalizing signal intensity of each time point to the signal intensity at time 0.

REFERENCES

1. Ilinskaya, A. N. & Dobrovolskaia, M. A. Immunosuppressive and anti-inflammatory properties of engineered nanomaterials. *Br. J. Pharmacol.* **171**, 3988–4000 (2014).

2. Lupus facts and statistics. (2018). Available at: https://resources.lupus.org/entry/facts-and-statistics.

3. Roper, G. *Executive Summary Lupus Awareness Survey October 2012 GfK Roper Public Affairs & Corporate Communications*. (2012).

4. Pons-Estel, G. J., Alarcón, G. S., , Lacie Scofield, L. & Reinlib, G. S. C. Understanding the Epidemiology and Progression of Systemic Lupus Erythematosus. *Semin Arthritis Rheum* **39**, 1–23 (2010).

5. Maidhof, W. & Hilas, O. Lupus: an overview of the disease and management options. *P T* **37**, 240–9 (2012).

6. Wallace, D. J. & Hahn, B. H. *Dubois' lupus erythematosus and related syndromes*. (Elsevier Saunders, 2013).

7. AL Sawah, S. *et al.* Understanding Delay in Diagnosis, Access to Care and Satisfaction with Care in Lupus: Findings from a Cross-Sectional Online Survey in the United States. in *Eurorpean League Against Rheumatism* (2015). doi:10.1136/annrheumdis-2015-eular.5063

8. Tsokos, G. C. Systemic Lupus Erythematosus. *N. Engl. J. Med.* **365**, 2110–2121 (2011).

9. Blair, H. A. & Duggan, S. T. Belimumab: A Review in Systemic Lupus Erythematosus.

Drugs **78**, 355–366 (2018).

10. Touma, Z. & Gladman, D. D. Current and future therapies for SLE: obstacles and recommendations for the development of novel treatments. *Lupus Sci. Med.* **4**, e000239 (2017).

11. Allen, C. D. C., Okada, T. & Cyster, J. G. Germinal Center Organization and Cellular Dynamics Christopher. *Immunity* **27**, 190–202 (2007).

12. Victoria, G. D. & Nussenzweig, M. C. Germinal Centers. *Annu. Rev. immunolo* **30**, 429–457 (2012).

13. Nutt, S. & Tarlinton, D. Germinal center B and follicular helper T cells: siblings, cousins or just good friends? *Nat. Immunol.* **12**, (2011).

14. Grammer, A. C. *et al.* Abnormal germinal center reactions in systemic lupus erythematosus demonstrated by blockade of CD154-CD40 interactions. *J. Clin. Invest.* **112**, 1506–1520 (2003).

15. Schroeder, H. W. & Cavacini, L. Structure and Function of Immunoglobulins. *J. Allergy Clin. Immunol.* **125**, S41–S52 (2010).

16. Hickey, J. W., Kosmides, A. K. & Schneck, J. P. Engineering Platforms for T Cell Modulation. *Int. Rev. Cell Mol. Biol.* **341**, 277–362 (2018).

17. Xie, Y. *et al.* Targeted Delivery of siRNA to Activated T Cells via Transferrin-Polyethylenimine (Tf-PEI) as a Potential Therapy of Asthma. doi:10.1016/j.jconrel.2016.03.029

18. Tyrrell, Z. L., Shen, Y. & Radosz, M. Fabrication of micellar nanoparticles for drug

delivery through the self-assembly of block copolymers. *Prog. Polym. Sci.* **35**, 1128–1143 (2010).

19. Ding, Q. *et al.* Targeting and liposomal drug delivery to CD40L expressing T cells for treatment of autoimmune diseases. *J. Control. Release* **207**, 86–92 (2015).

20. Wang, Y., Qu, W. & Choi, S. FDA's Regulatory Science Rogram for Generic PLA/PLGA-Based Drug Products. *American Pharmaceutical Review* (2016). Available at: https://www.americanpharmaceuticalreview.com/Featured-Articles/188841-FDA-s-Regulatory-Science-Program-for-Generic-PLA-PLGA-Based-Drug-Products/.

21. Smelkinson, M. The Hedgehog Signaling Pathway Emerges as a Pathogenic Target. *J. Dev. Biol.* **5**, 14 (2017).

22. Crompton, T., Outram, S. V. & Hager-Theodorides, A. L. Sonic hedgehog signalling in T-cell development and activation. *Nat. Rev. Immunol.* **7**, 726–735 (2007).

23. Chan, V. S. F. *et al.* Sonic hedgehog promotes CD4+T lymphocyte proliferation and modulates the expression of a subset of CD28-targeted genes. *Int. Immunol.* **18**, 1627–1636 (2006).

24. Riley, J. L. & June, C. H. The CD28 family: A T-cell rheostat for therapeutic control of T-cell activation. *Blood* **105**, 13–21 (2005).

25. Sacedon, R. *et al.* Sonic Hedgehog Is Produced by Follicular Dendritic Cells and Protects Germinal Center B Cells from Apoptosis. *J. Immunol.* **174**, 1456–1461 (2005).

26. Koncz, G. & Hueber, A. O. The Fas/CD95 receptor regulates the death of autoreactive B cells and the selection of antigen-specific B cells. *Front. Immunol.* **3**, 1–12 (2012).

27. Williams, C. H. *et al.* An In vivo Chemical Genetic Screen Identifies Phosphodiesterase 4 as a Pharmacological Target for Hedgehog signaling Inhibition Charles. *Cell Rep.* **11**, 43–50 (2015).

28. McHugh, M. D. *et al.* Paracrine co-delivery of TGF-β and IL-2 using CD4-targeted nanoparticles for induction and maintenance of regulatory T cells. *Biomaterials* **59**, 172–181 (2015).

29. Chinol, M. *et al.* Biochemical modifications of avidin improve pharmacokinetics and biodistribution, and reduce immunogenicity. *Br. J. Cancer* **78**, 189–197 (1998).

30. Song, G., Petschauer, J., Madden, A. & Zamboni, W. Nanoparticles and the Mononuclear Phagocyte System: Pharmacokinetics and Applications for Inflammatory Diseases. *Curr. Rheumatol. Rev.* **10**, 22–34 (2014).

31. Cao, S. *et al.* Optimization and comparison of CD4-targeting lipid–polymer hybrid nanoparticles using different binding ligands. *J. Biomed. Mater. Res. - Part A* **106**, 1177–1188 (2018).

32. ThermoFisher. Lipophilic Tracers. 1–6 (2008). Available at: https://www.thermofisher.com/order/catalog/product/D7757.

33. Sah, H., Thoma, L. A., Desu, H. R., Sah, E. & Wood, G. C. Concepts and practices used to develop functional PLGA-based nanoparticulate systems. *Int. J. Nanomedicine* **8**, 747–765 (2013).

34. ThermoFisher. Pierce ™ Fab Preparation Kit. doi:10.1002/(SICI)1097-0118(199906)31:2<107::AID-JGT4>3.0.CO;2-L

35. Li, S.-D. & Huang, L. Pharmacokinetics and biodistribution of nanoparticles. *Mol Pharm* **5**, 496–504 (2008).

36. Moghimi, S. M., Hunter, A. C. & Andresen, T. L. Factors Controlling Nanoparticle Pharmacokinetics: An Integrated Analysis and Perspective. *Annu. Rev. Pharmacol. Toxicol.* **52**, 481–503 (2012).

37. Hoshyar, N., Gray, S., Han, H. & Bao, G. The effect of nanoparticle size on in vivo pharmacokinetics and cellular interaction. *Nanomedicine* **11**, 673–692 (2016).

38. Schmid, D. *et al.* T cell-targeting nanoparticles focus delivery of immunotherapy to improve antitumor immunity. *Nat. Commun.* **8**, 1–11 (2017).

39. Honary, S. & Zahir, F. Effect of Zeta Potential on the Properties of Nano-Drug Delivery Systems - A Review (Part 1). *Trop. J. Pharm. Res.* **12**, 255–264 (2013).

40. Fröhlich, E. The role of surface charge in cellular uptake and cytotoxicity of medical nanoparticles. *Int. J. Nanomedicine* **7**, 5577–5591 (2012).

41. Olivier, J. C., Huertas, R., Hwa, J. L., Calon, F. & Pardridge, W. M. Synthesis of pegylated immunonanoparticles. *Pharm. Res.* **19**, 1137–1143 (2002).

42. Hong, C. *et al.* Compounds and Methods for Inhibiton of Hedgehog Signaling and Phosphodiesterase. (2016).

43. Dinarvand, R., Sepehri, N., Manoochehri, S., Rouhani, H. & Atyabi, F. Polylactide-co-glycolide nanoparticles for controlled delivery of anticancer agents. *Int. J. Nanomedicine* **6**, 877–895 (2011).

44. Hirenkumar K. Makadia1 and Steven J. Siegel2, H. Poly Lactic-co-Glycolic Acid (PLGA)

as Biodegradable Controlled Drug Delivery Carrier Hirenkumar. *Polym.* **3**, 1377–1397 (2011).

45. Jackson, S. *et al.* B cell IFN-γ receptor signaling promotes autoimmune germinal centers via cell-intrinsic induction of BCL-6. *J. Exp. Med.* **213**, 733–750 (2016).

46. Ernsting, M. J., Murakami, M., Roy, A. & Li, S. D. Factors controlling the pharmacokinetics, biodistribution and intratumoral penetration of nanoparticles. *J. Control. Release* **172**, 782–794 (2013).

47. Miteva, M. *et al.* Tuning PEGylation of mixed micelles to overcome intracellular and systemic siRNA delivery barriers. *Biomaterials* **38**, 97–107 (2015).